Structure and Mechanism of *Pseudomonas aeruginosa* PhzD, an Isochorismatase from the Phenazine Biosynthetic Pathway[†,‡,§]

James F. Parsons,[||] Kelly Calabrese,[||] Edward Eisenstein,*[,||,⊥] and Jane E. Ladner*[,||]

Center for Advanced Research in Biotechnology, University of Maryland Biotechnology Institute, National Institute of Standards and Technology, 9600 Gudelsky Drive, Rockville, Maryland 20850, and Department of Chemistry and Biochemistry, University of Maryland Baltimore County, Baltimore, Maryland 21228

Received December 20, 2002; Revised Manuscript Received March 14, 2003

ABSTRACT: PhzD from *Pseudomonas aeruginosa* is an isochorismatase involved in phenazine biosynthesis. Phenazines are antimicrobial compounds that provide *Pseudomonas* with a competitive advantage in certain environments and may be partly responsible for the persistence of *Pseudomonas* infections. In vivo, PhzD catalyzes the hydrolysis of the vinyl ether functional group of 2-amino-2-deoxyisochorismate, yielding pyruvate and *trans*-2,3-dihydro-3-hydroxyanthranilic acid, which is then utilized in the phenazine biosynthetic pathway. PhzD also catalyzes hydrolysis of the related vinyl ethers isochorismate, chorismate, and 4-amino-4-deoxychorismate. Here we report the 1.5 Å crystal structure of native PhzD, and the 1.6 Å structure of the inactive D38A variant in complex with isochorismate. The structures reveal that isochorismate binds to the PhzD active site in a *trans*-diaxial conformation, and superposition of the structures indicates that the methylene pyruvyl carbon of isochorismate is adjacent to the side chain carboxylate of aspartate 38. The proximity of aspartate 38 to isochorismate and the complete loss of activity resulting from the conversion of aspartate 38 to alanine suggest a mechanism in which the carboxylate acts as a general acid to protonate the substrate, yielding a carbocation/oxocarbonium ion that is then rapidly hydrated to form a hemiketal intermediate, which then decomposes spontaneously to products. The structure of PhzD is remarkably similar to other structures from a subfamily of α/β-hydrolase enzymes that includes pyrazinamidase and *N*-carbamoylsarcosine amidohydrolase. However, PhzD catalyzes unrelated chemistry and lacks a nucleophilic cysteine found in its close structural relatives. The vinyl ether hydrolysis catalyzed by PhzD represents yet another example of the catalytic diversity seen in the α/β-hydrolase family, whose members are also known to hydrolyze amides, phosphates, phosphonates, epoxides, and C−X bonds.

Pyocyanin, phenazine-1-carboxylic acid (Scheme 1), and more than 70 related compounds collectively known as phenazines are bioactive metabolites produced by various species of *Pseudomonas*, including the human pathogen *Pseudomonas aeruginosa* (*1*−*4*). Phenazines exhibit antimicrobial activity that provides *Pseudomonas* with a competitive advantage in certain environments and may enhance their potential as opportunistic pathogens in humans and other animals. Usher et al. (*5*) have demonstrated that pyocyanin can induce death in human neutrophils, and the authors suggest that this may be a factor in the persistence of *P. aeruginosa* infections of human tissue. The activity associated with phenazines has been proposed to be a consequence of superoxide, peroxide, and hydroxyl radical production resulting from oxidation−reduction processes in which phenazines participate (*3*, *5*−*7*). Pyocyanin has also been directly implicated in the inactivation of α_1 protease inhibitor, potentially contributing to the protease-mediated injury seen in lungs of patients infected with *P. aeruginosa* (*8*).

Chorismic acid has been shown to be a precursor for phenazine biosynthesis, and two operons containing seven genes involved in phenazine biosynthesis (*phzABCDEFG*) have been identified in *P. aeruginosa*. Each of these operons encodes all of the genes required to produce phenazine-1-carboxylic acid from chorismate (*3*), and tentative functional assignments have been proposed for some of these gene products (*4*). BLAST (*9*) analysis indicates PhzE is similar to bacterial anthranilate synthases, which catalyze the related conversion of chorismate to anthranilate. However, unlike anthranilate synthase, which sequesters an aminodeoxyisochorismate (ADIC)[1] intermediate, ADIC is the final product

[†] This work was supported in part by National Science Foundation Grant MCB 23086 (to E.E.).

[‡] Certain commercial materials, instruments, and equipment are identified in this paper to specify the experimental procedure as completely as possible. In no case does such identification imply a recommendation or endorsement by the National Institute of Standards and Technology, nor does it imply that the materials, instruments, or equipment identified is necessarily the best available for the purpose.

[§] Coordinates for native PhzD and D38A PhzD in complex with isochorismate have been deposited in the RCSB Protein Data Bank as entries 1NF9 and 1NF8, respectively.

* To whom correspondence should be addressed: Center for Advanced Research in Biotechnology, 9600 Gudelsky Dr., Rockville, MD 20850. E-mail: jane.ladner@nist.gov or edd@carb.nist.gov.

[||] National Institute of Standards and Technology.

[⊥] University of Maryland Baltimore County.

[1] Abbreviations: ADIC, 2-amino-2-deoxyisochorismate; DHHA, *trans*-2,3-dihydro-3-hydroxyanthranilic acid; ACP, aryl carrier protein; ADC, 4-amino-4-deoxychorismate; CSHase, *N*-carbamoylsarcosine amidohydrolase; PZAase, pyrazinamidase.

10.1021/bi027385d CCC: $25.00
Published on Web 04/25/2003

Scheme 1

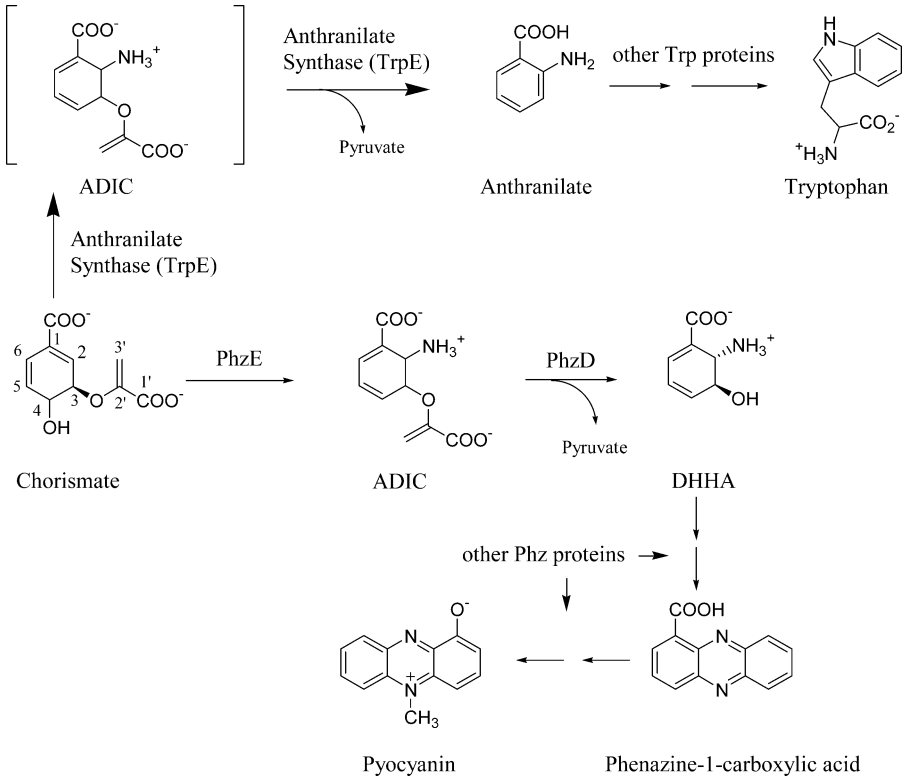

of the PhzE-catalyzed transformation of chorismate (Scheme 1). Biochemical evidence has shown that PhzD catalyzes the conversion of ADIC to *trans*-2,3-dihydro-3-hydroxyanthranilic acid (DHHA) (*4*). DHHA is then converted to phenazine-1-carboxylic acid in several poorly characterized steps, probably involving the condensation of two DHHA molecules to form the phenazine ring system. Additionally, PhzD is 46% identical to the EntB isochorismatase from *Escherichia coli*, but PhzD lacks the C-terminal aryl carrier protein (ACP) domain found in EntB. This ACP domain has an additional role unique to the enterobactin synthetic pathway and is unrelated to the isochorismatase activity (*10*, *11*).

The reaction catalyzed by PhzD and related isochorismatase enzymes is the hydrolysis of a vinyl ether, an uncommon reaction in biological systems. The only other known examples are the reactions catalyzed by alkenyl ether hydrolases, microsomal enzymes found in most mammalian cells (*12*−*14*). Although the chemical mechanism of vinyl ether hydrolysis is well-characterized (*15*), the role of the enzyme remains unclear.

As part of an effort to understand the molecular basis for the interesting similarities and striking differences seen in chorismate-utilizing enzymes, this work describes the 1.5 Å resolution crystal structure of PhzD and the 1.6 Å resolution structure of the inactive D38A variant of PhzD in complex with isochorismate. Structural and biochemical analysis confirms that PhzD is an isochorismatase that preferentially utilizes ADIC, and can also act on aminodeoxychorismate (ADC), chorismate, and isochorismate as substrates. The structure of PhzD is remarkably similar to other structures from a subfamily of α/β-hydrolase enzymes that includes pyrazinamidase (PZAase) (*16*) and *N*-carbamoylsarcosine amidohydrolase (CSHase) (*17*), both of which catalyze amide hydrolysis reactions via a catalytic triad featuring a cysteine nucleophile. PhzD differs from these enzymes substantially, however, in terms the type of chemistry it catalyzes and the identity and role of key active site residues. The isochorismate-bound structure, as well as the properties of the D38A variant, suggests a mechanism by which PhzD facilitates vinyl ether hydrolysis and provides the first view of isochorismate bound to an enzyme active site. Additionally, the PhzD−isochorismate complex yields important clues about the binding of other chorismate-like molecules to related enzymes in this highly conserved yet functionally distinct family of enzymes.

MATERIALS AND METHODS

Cloning. The DNA encoding PhzD was amplified from *P. aeruginosa* genomic DNA (ATCC) using synthetic primers that are compatible with the *phzD* (PA1902) sequence as described in the TIGR Comprehensive Microbial Resource database (www.tigr.org). *Nde*I and *Hin*dIII restriction enzyme sites were included in the primers, and the digested fragment was ligated into the similarly digested expression vector pET-28a (Novagen).

Mutagenesis. Complementary DNA primers containing either the D38A or K122A mutation, and a silent mutation encoding a restriction enzyme site for diagnostic purposes, were purchased commercially, and the mutant clones were isolated using the QuikChange (Stratagene) protocol as described by the manufacturer. Mutations were confirmed by DNA sequencing.

Protein Expression and Purification. P. aeruginosa PhzD was expressed in *E. coli* strain BL21(DE3). Cells harboring the pET28a-PhzD plasmid were grown in shaker flasks at 37 °C to a density of 1.0 at 600 nm in LB medium containing 100 μg/mL ampicillin, and protein production was induced

by addition of IPTG to a final concentration of 1 mM. Growth was continued for 3 h, at which time cells were harvested by centrifugation. Cells were lysed by sonication. Extracts containing PhzD were processed using Ni−NTA affinity resin (Novagen) as directed by the manufacturer. Fractions containing pure PhzD, as judged by sodium dodecyl sulfate−polyacrylamide gel electrophoresis, were pooled, concentrated to approximately 10 mg/mL, and dialyzed against 50 mM Tris-HCl, 0.1 M NaCl, 1 mM DTT, and 1 mM EDTA (pH 8.0). Human thrombin (~0.5 μg/mg of PhzD; Haematologic Technologies) was then added, and the mixture was incubated at room temperature for 1 h before being applied to a benzamidine agarose (Sigma) column with a second Ni−NTA agarose column attached in series to capture the thrombin and the cleaved hexahistidine affinity tag, respectively. PhzD-containing fractions were then dialyzed against 50 mM MOPS, 1 mM DTT, and 1 mM EDTA (pH 7.2), concentrated to 17 mg/mL, and stored at −80 °C. The D38A and K122A mutants were expressed and purified in an identical manner, and yields for all were ~40 mg of pure enzyme per liter of culture.

Crystallization. Crystals of both native PhzD and the D38A variant were grown from hanging drops by vapor diffusion at room temperature. The protein solution contained ~17 mg/mL PhzD in the buffer described above, and 0.2% β-octyl glucoside. To obtain quality crystals, it was also necessary to include a substrate in the mixture. For native PhzD, either 1 mM ADIC or 1 mM ADC was included, whereas 1 mM isochorismate was included in the D38A variant crystallization trials. The protein solution was mixed with an equal volume of 10% polyethylene glycol 4000 and 0.2 M ammonium formate, and 4 μL drops were equilibrated against wells containing 10−20% polyethylene glycol 4000 and 0.2 M ammonium formate. Crystals appeared in 1−3 days and were variable in size.

Data Collection. Diffraction data were collected using a Rigaku Micro Max 007 rotating anode generator and a Rigaku RAXIS IV^{++} detector (Rigaku/MSC, The Woodlands, TX). The crystals were cooled to 100 K with a Rigaku Xtream 2000 cryocooler and were cryoprotected by the addition of 50% polyethylene glycol 4000 to the reservoir solution in a ratio of 1:1. Diffraction data were collected and processed with CrystalClear/d*Trek (*18*). Statistics for the data collection and refinement are shown in Table 1.

Structure Determination. Initial attempts to determine the structure by molecular replacement were not successful. Alternatively, since PhzD was able to bind various mercurial compounds in solution as seen by MALDI mass spectrometry using a Voyager-DE spectrometer (PerSeptive Biosystems), an attempt was made to make a mercury derivative for phasing. A crystal was soaked briefly in a solution of ethylmercury phosphate, and data were collected to 1.4 Å. Analysis of the data did not indicate the presence of mercury; there was only a small anomalous component, and attempts to find sites using single isomorphous replacement and single anomalous dispersion with mercury failed. However, the program SOLVE (*19*; www.solve.lanl.gov) found 10 sites initially thought to be from the seven cysteine and three methionine residues in the primary sequence when analyzing the data with the *f″* value for sulfur. Using these sites, the program RESOLVE (*20*, *21*) was able to build 120 of 207 residues and place 69 side chains using the known sequence of PhzD. Iterative application of RESOLVE (without refinement) increased the completeness of the model to 196 residues with 191 side chains placed.

Table 1: Data Collection and Refinement Statistics

	native PhzD	D38A PhzD
diffraction data		
space group	$C222_1$	$C222_1$
cell dimensions (*a*, *b*, *c*) (Å)	68.85, 77.03, 82.55	68.40, 77.01, 82.44
resolution (Å)	1.5	1.6
no. of measured intensities	357616	82842
no. of unique reflections	33819	27572
mean redundancy	11	3
R_{merge} (overall/high-resolution shell)	0.032/0.097	0.042/0.207
completeness (overall/high-resolution shell)	92.7/80.4	99.7/99.0
average I/σ (overall/high-resolution shell)	25.6/3.2	22.0/3.1
refinement		
resolution limits (Å)	20.0−1.5	20.0−1.6
R-factor (95% of the data)	0.155	0.134
R_{free} (5% of the data)	0.225	0.210
no. of non-protein molecules (not water)	formate ion, β-octyl glucoside	isochorismate, β-octyl glucoside
no. of water molecules	291	298
bond length rms deviation (Å)	0.010	0.008
angle distance rms deviation (Å)	0.031	0.026
average *B* (main chain/side chain) (Å^2)	17.3/23.2	16.0/21.7
average *B* for water (Å^2)	35.9	33.8

Analysis of the original "sulfur" sites after the complete tracing of the polypeptide chain showed that two of the original sites were not due to Met or Cys residues in the protein, but were near H130 and H184. It is likely that these are very low occupancy mercury sites. Met1 and Met187 did not give an anomalous signal.

SHELX (*22*) was used to refine the structure against the diffraction data, and the structure was verified using PROCHECK (*23*). REDUCE and PROBE (*24*) were used to guide rebuilding to help resolve side chain conformations. XTALVIEW (*25*) was used to examine and adjust the molecule to fit the electron density visually. Refinement statistics are presented in Table 1. DALI (*26*) (http://www2.ebi.ac.uk/dali/) and CE (*27*) (http://cl.sdsc.edu) were used for automated structural superposition of PhzD against the Protein Data Bank (*28*).

Synthesis of ADIC, ADC, and Isochorismate. ADC was synthesized as previously described (*29*). Isochorismate was synthesized as described by Rusnak et al. (*30*) except that the *E. coli* MenF isochorismate synthase was used. ADIC was prepared essentially as described by Morollo et al. (*31*) with some minor differences. Chorismic acid (25 mg) was dissolved in 15 mL of 300 mM ammonium carbonate and 5 mM $MnCl_2$ (pH 8.2). The H398M variant of *Salmonella typhimurium* anthranilate synthase was added to a final concentration of approximately 20 μM (*32*). The reaction was monitored by HPLC until equilibrium was reached (~3.5 h), at which time the reaction mixture was extracted with

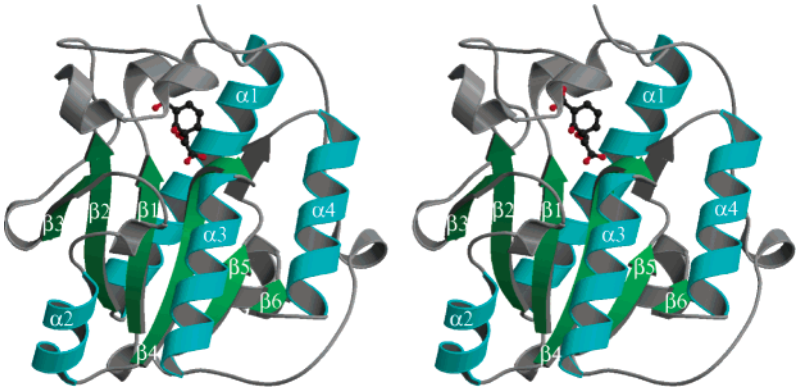

FIGURE 1: Stereo ribbon diagram of D38A PhzD in complex with isochorismate. Major secondary structural elements are labeled. This figure was prepared using XTALVIEW and RASTER3D.

three 15 mL portions of chloroform and then three 15 mL portions of ethyl acetate. The aqueous portion containing ADIC was then lyophilized, redissolved in 1 mL of 5% acetic acid, and subjected to HPLC (Waters μbondapak C18 column, 7.8 mm × 300 mm, 4 mL/min) using a mobile phase of 5% acetic acid. ADIC-containing fractions were pooled and lyophilized three times from H_2O. Purified ADIC was stored in solution (~25 mM) at −80 °C.

Molecular Mass from Laser Light Scattering. The solution molecular mass of PhzD was determined by a combination of laser light scattering and interferometric refractometry using a DAWN EOS and Optilab DSP system (Wyatt). Filtered samples were subjected to gel filtration chromatography (Pharmacia Superdex 75, 200 mm × 5 mm) prior to in-line analysis. Molecular masses were calculated using ASTRA software.

Measurement of Enzymatic Activity. Two methods were used to monitor the PhzD-catalyzed conversion of ADIC to DHHA and pyruvate. Formation of DHHA was followed directly by HPLC (λ = 272 nm; Waters Xterra C18 column, 4.6 mm × 100 mm) using a mobile phase of 5% acetic acid and a flow rate of 0.8 mL/min (*31*). Under these conditions, ADIC elutes at approximately 8 min and DHHA at approximately 3.2 min. A continuous spectrophotometric assay using lactate dehydrogenase was employed essentially as described to determine kinetic constants for the enzyme using ADIC, ADC, chorismate, and isochorismate as substrates (*30*). Assays were performed at pH 6.5 in 0.1 M Bis-Tris. Crystals of PhzD were recovered from hanging drops, rinsed, and then added to fresh ~10 μL drops of well solution containing substrate to assay for product formation using HPLC.

Determination of Ligand Dissociation Constants Using Fluorescence Spectroscopy. Steady-state emission spectra from 305 to 400 nm were recorded at pH 6.5 in 0.1 M Bis-Tris on a Spex Fluoromax fluorimeter maintained at 25 °C by a circulating water bath. An excitation wavelength of 295 nm was used. Protein concentrations for binding experiments ranged from 100 to 500 nM depending on the ligand used as the titrant. Values for the dissociation constants were determined from the significant decrease in tryptophan fluorescence at 340 nm as a function of the concentration of ligand. The data were fit to a hyperbola in the case of chorismate or to a quadratic function (eq 1) for ADIC and isochorismate ([L]) where A represents the titration amplitude, S the offset from zero, and [P] the monomer concentration of PhzD.

$$\Delta F = S + \frac{A[1 - (K_d + [P] + [L]) - (\sqrt{(K_d + [P] + [L])^2 - 4[P][L]})]}{2[P]} \quad (1)$$

The extent of chorismate binding to the D38A variant of PhzD was also determined by rapid kinetic methods. D38A PhzD (500 nM) was rapidly mixed with various concentrations of chorismate under pseudo-first-order conditions using an Applied PhotoPhysics SX17 stopped flow spectrometer thermostated at 25 °C. An excitation wavelength of 295 nm was used, and the total fluorescence was measured through a 320 nm cutoff filter. The fluorescence quenching measured upon chorismate binding was recorded, and the data were fit to an equation describing a single-exponential decay to obtain an observed rate constant. At least five traces were averaged for each concentration of chorismate that was used. The observed rate constants were then plotted against chorismate concentration, and the data were fit to a linear function (eq 2). The equilibrium dissociation constant, K_d, was calculated from eq 3.

$$k_{obs} = k_{on}[\text{chorismate}] + k_{off} \quad (2)$$

$$K_d = k_{off}/k_{on} \quad (3)$$

RESULTS

Overall Structure. The PhzD polypeptide folds into a single α/β domain with three helices packed on one side of a six-stranded parallel β-sheet and a single long helix on the other side of the sheet (Figures 1 and 3). The order of the strands in the sheet is 3-2-1-4-5-6 relative to the primary sequence. A 32-residue, mainly random, N-terminal coil wraps around the molecule and closes over the active site (Figure 3). PhzD crystallized in space group $C222_1$ with one polypeptide chain in the asymmetric unit. In solution, however, PhzD is a dimer. Light scattering indicates a molecular mass of 49 400 ± 1100 Da, or approximately twice the monomer mass for the polypeptide chain of 23 478 Da. Additionally, 2740 Å^2 of buried surface area with a 2-fold crystallographic mate is likely the physiologic dimer inter-

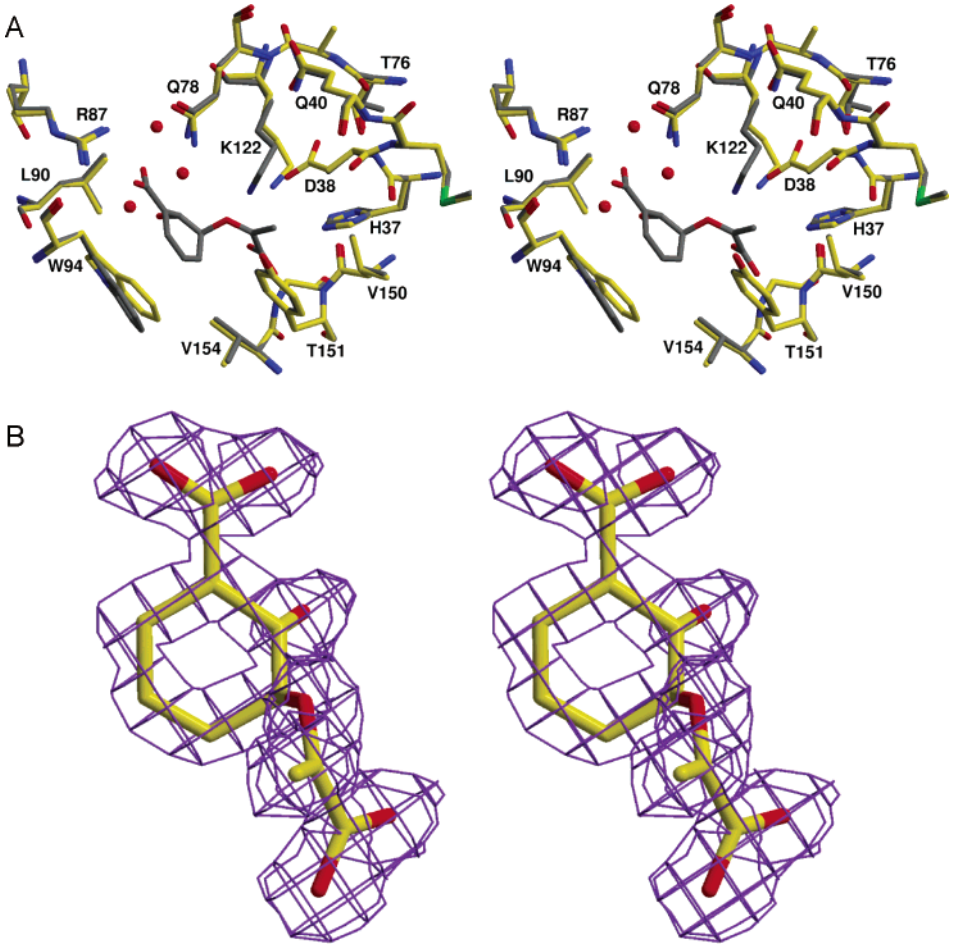

FIGURE 2: (A) Stereoview of the active site of *P. aeruginosa* PhzD. The D38A structure (carbon atoms shown in gray) is superimposed on the native structure (carbon atoms shown in yellow). Isochorismate from the D38A structure is shown along with the active site water molecules found in that structure. The two water molecules near the front of the figure are found in both structures. (B) Stereoview of isochorismate with positive omit map electron density. After 10 cycles of refinement in which the isochorismate molecule was omitted, sigmaA weighted ($F_o - F_c$) density was calculated and is shown contoured at 3σ. This figure was prepared using XTALVIEW and RASTER3D.

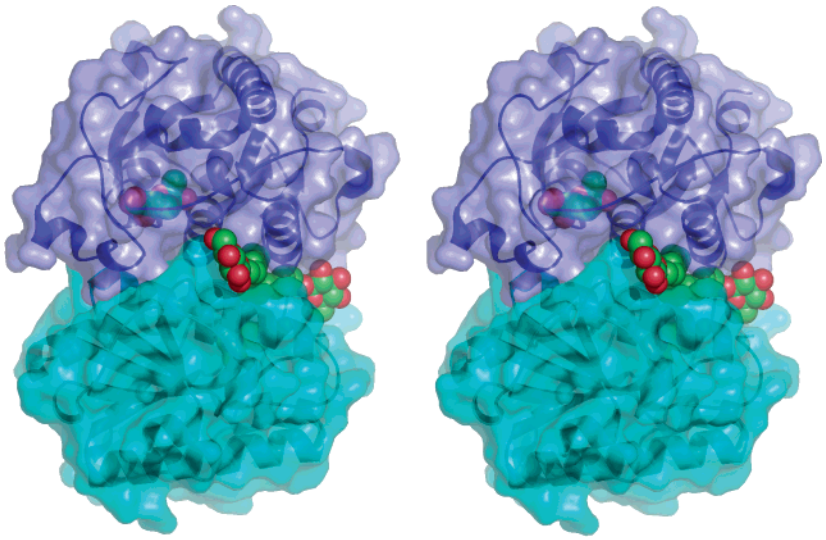

FIGURE 3: Stereo ribbon diagram of the PhzD dimer with a semitransparent surface. The bound isochorismate molecule is shown in the buried active site as space-filling atoms. The N-terminus of the protein can be seen covering a possible route of ingress to and egress from the active site. Two bound β-octyl glucoside detergent molecules are shown as space-filling molecules with their polar headgroups protruding from the protein surface and their lipid tails buried in the protein interior. This figure was generated using PyMOL (www.pymol.org).

face. Two molecules of β-octyl glucoside, necessary for the crystallization of PhzD, can be seen at the dimer interface with their hydrophobic tails embedded between the two monomers. The crystals diffracted quite well, and density is seen for the entire polypeptide chain except for the N-terminal Gly-Ser-His extension remaining after thrombin

Scheme 2

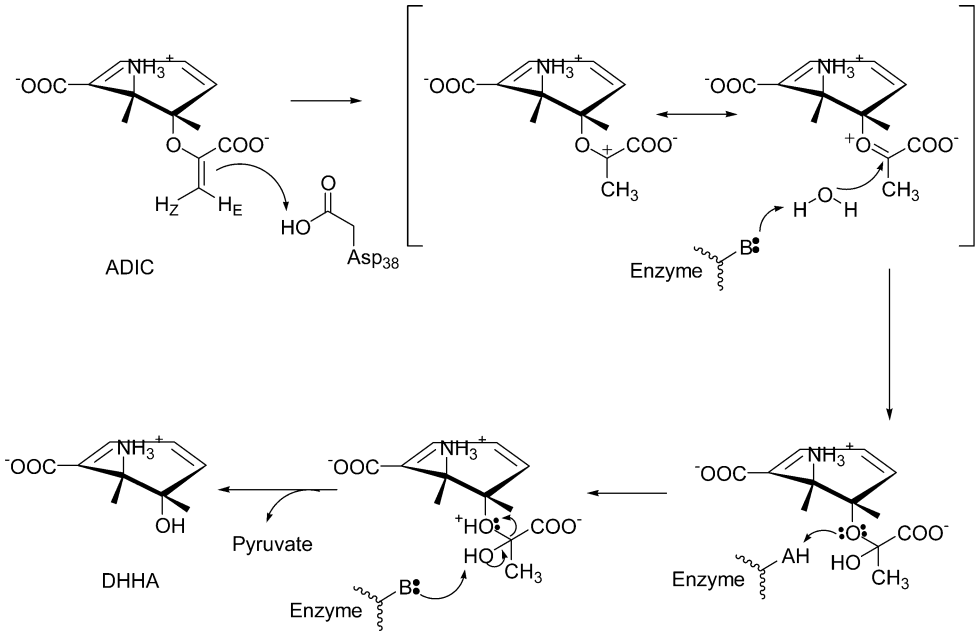

Table 2: Results of DALI Search for Protein Structures Similar to PhzD

PDB entry	protein	DALI *Z* score	rmsd (Å)	no. of aligned residues	% sequence identity
1IM5	pyrazinamidase	22.6	1.6	141	23
1NBA	*N*-carbamoylsarcosine amidohydrolase	21.2	2.0	145	13
1YAC	hydrolase, unknown specificity	19.6	2.1	154	20

cleavage. These residues are therefore not included in the model. A few residues on the surface of the molecule show increased *B* values for the side chain atoms. The Ramachandran plot highlights a single residue (V154) in the "generously allowed region". A *cis* peptide bond is observed between residues Y150 and V151.

The native PhzD and D38A structures are essentially identical aside from the mutation. The crystals were of the same space group, had similar unit cell parameters, and grew from the same conditions. The rmsd between the two structures is 0.24 Å for backbone atoms and 0.46 Å for all non-hydrogen atoms of residues 2−206. The most significant changes are in the side chain conformations of active site residues K122 and W94 (Figure 2). Several other surface residues show significant deviations ($>2\sigma$), including R64, K91, E109, and N135.

Active Site. The active site of PhzD is buried at the C-terminal end of the β-sheet and near the dimer interface (Figures 2A and 3). The N-terminus of the protein and residues 78−104, which lie between β2 and β3, contribute to a significantly occluded active site (Figure 3). The structure of the complex between isochorismate and the D38A variant of PhzD permits identification of the residues that interact directly with the bound substrate. Isochorismate is bound in a *trans* diaxial conformation (Figure 2A). Clear density was observed for the entire substrate molecule (Figure 2B). A combination of hydrogen bonds and hydrophobic interactions tethers isochorismate to the active site. A hydrophobic pocket consisting of I4, W94, F43, Y125, Y151, L154, and F180 surrounds the nonpolar portion of the cyclohexadiene ring of the substrate. The ring carboxylate of the substrate forms hydrogen bonds with the side chains of Q78 and R87, and the pyruvyl carboxylate is hydrogen bonded to the main chain amides of G155 and Y151, and the ϵ-amino group of K122. The *re* face of C2′ of isochorismate is oriented toward A38 of the mutant, and C3′ is within 3.1 Å of D38 Oδ2 when the structures are superimposed, suggesting that protonation of the substrate occurs specifically on one face of methylene C3′. This face can arbitrarily be assigned as *re* if the C3′ protons are designated H_Z and H_E, where H_E is of greater priority than H_Z, as shown in Scheme 2. Interestingly, diffraction quality crystals of native PhzD were only obtained in the presence of ADC, yet no interpretable density for ADC or either product was observed in the active site. Instead, several water molecules and a formate ion occupy the space in this region. The formate ion occupies a position near R87 and Q78, adjacent to the location of the ring carboxyl of isochorismate in the D38A structure (Figure 2A). Enzyme assays showed not only that PhzD retains activity in the crystallization mixture but also that the crystals themselves are catalytically active.

Structure Relatives. Automated superposition of PhzD using the program DALI (*26*) revealed significant similarity to three known structures (Table 2). *N*-Carbamoylsarcosine amidohydrolase (*17*) and pyrazinamidase (*16*) are hydrolases known to use a cysteine nucleophile, and YcaC likely does as well, although its substrate is unknown (*33*). Isochorismatases, including PhzD, have a glycine at the analogous position (G155), suggesting a nucleophile is not involved in vinyl ether hydrolysis. The quaternary structures of the related molecules mentioned above vary considerably. PZAase is a monomer, CSHase a tetramer, and 1YAC an octamer. Interestingly, the dimeric arrangement of the PhzD monomer is equivalent to the AB and CD dimers seen in CSHase (*17*), although the tetramer and octamer do not have similar interfaces.

Table 3: Kinetic Constants for PhzD toward Various Substrates

	k_{cat}[a] (s^{-1})	K_m (μM)	k_{cat}/K_m (M^{-1} s^{-1})	K_d[b] (μM)
ADIC	7.3 ± 0.2	68 ± 5	$(1.1 \pm 0.1) \times 10^5$	0.021 ± 0.001
isochorismate	0.2 ± 0.03	4 ± 2	$(5.0 \pm 4) \times 10^4$	0.015 ± 0.01
ADC	0.02 ± 0.002	590 ± 140	$(3.4 \pm 2.4) \times 10^1$	nd[c]
chorismate	1.2 ± 0.06	983 ± 77	$(1.2 \pm 0.2) \times 10^3$	19 ± 2
				13 ± 3[d]

[a] Kinetic constants for native PhzD determined by a coupled spectrophotometric assay with lactate dehydrogenase as described in Materials and Methods. [b] Determined by fluorescence titration using the D38A variant. [c] Not determined. [d] Determined by stopped flow spectroscopy using the D38A variant.

Kinetic Analysis of PhzD-Catalyzed Vinyl Ether Hydrolysis. Chorismate-utilizing enzymes exhibit promiscuity with respect to substrate binding and catalysis (*30*, *34*). Kinetic parameters of PhzD were therefore determined using four substrates, including the in vivo substrate ADIC, to glean information regarding the features of the substrate molecule that are important for recognition by PhzD. Values of k_{cat} and K_m for ADIC, ADC, chorismate, and isochorismate are presented in Table 3. The data show that PhzD hydrolyzes ADIC slightly more efficiently than it hydrolyzes isochorismate and considerably more efficiently than it hydrolyzes chorismate. ADC is a very poor substrate for PhzD and is barely hydrolyzed at all. The D38A variant exhibited no detectable activity toward any of the compounds listed in Table 3. In contrast, the K122A variant exhibited specific activities of 0.034 and 0.012 s^{-1} toward ADIC and isochorismate, respectively (100 μM in each case), suggesting it may have an important but not vital role in catalysis.

The strength of substrate binding was inferred from equilibrium and rapid kinetic experiments using the inactive D38A variant of PhzD. As can be seen in Figure 4 and Table 3, ADIC and isochorismate bind tightly to the D38A variant of PhzD, with dissociation constants of 10−20 nM, and it is likely that these ligands also bind strongly to wild-type PhzD (vida infra). Alternatively, chorismate, which has a substituent on C2 instead of C4, forms a substantially weaker complex with PhzD. As can be seen in Figure 5, the dissociation constant for chorismate binding to the D38A variant of PhzD is ~20 μM, some 1000-fold weaker than that for ADIC and isochorismate.

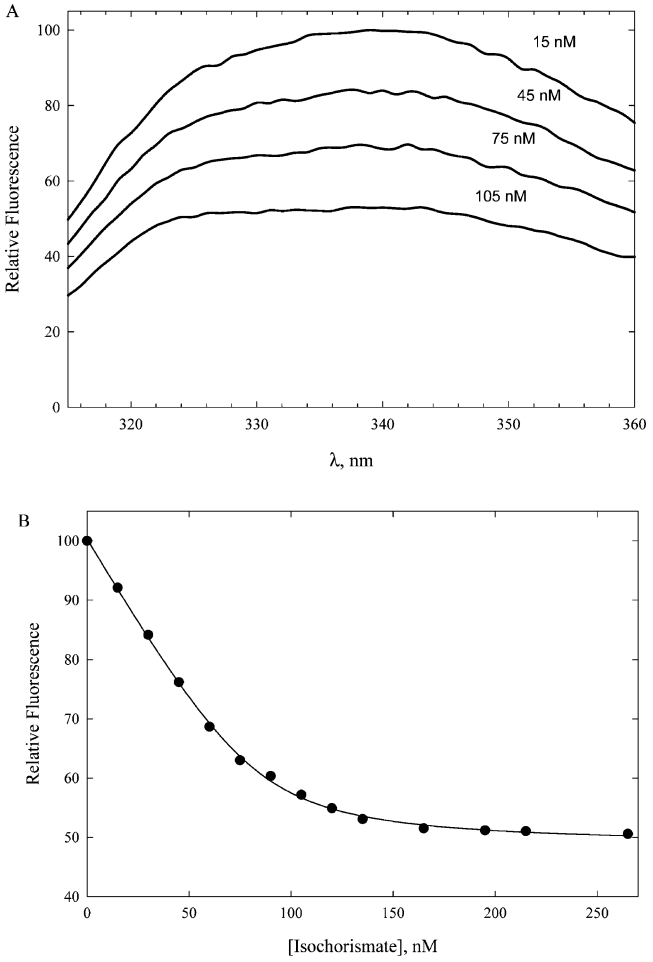

FIGURE 4: Effect of isochorismate on the fluorescence emission spectra of D38A PhzD. (A) Fluorescence emission spectra of D38A PhzD (100 nM) following the addition of isochorismate to final concentrations of 15, 45, 75, and 105 nM. (B) Equilibrium fluorescence intensity as a function of ligand concentration for isochorismate binding. Data were fit to eq 1 as described in Materials and Methods to determine K_d.

DISCUSSION

Vinyl ether hydrolysis, although well-characterized in solution, is uncommon in biological systems (*30*, *35*), and to date, no structure has been described for either an isochorismatase or any enzyme that catalyzes vinyl ether hydrolysis. Chorismic acid and the related compounds, isochorismate, ADIC, and ADC, are among the best-known vinyl ethers metabolized in biological systems, leading to a variety of important aromatic compounds (*36*). Numerous biochemical studies have led to a variety of mechanistic possibilities for enzymes acting on chorismate and related compounds (*32*, *36*−*38*), but a detailed proposal for the mechanism of chorismate-utilizing enzymes has been hampered in part due to a lack of readily interpretable structural data, particularly for enzyme−ligand complexes (*39*−*41*). The structures of ADC synthase and anthranilate synthase, for example, do not provide a complete picture of how chorismate binds to the active site of these proteins. Without this additional structural information, a detailed mechanistic interpretation is hampered, especially as chorismate in solution is an equilibrium mixture of conformers (*42*).

Structural data for PhzD and for the inactive D38A variant in complex with isochorismate show that PhzD binds the 2,3-*trans* diaxial conformation of isochorismate. Interestingly, it is the diequatorial conformer of chorismate and ADIC that has been shown to be the predominant species in solution, and it is reasonable to assume that the diequatorial conformation of isochorismate is also favored in solution (*31*, *42*). Therefore, either PhzD selectively binds the minor conformation from the solution population, or the substrate isomerizes after binding to the enzyme. Previous experiments indicate that the interconversion of the conformers of chorismate is rapid, suggesting that the enzyme has no need to isomerize the substrate (*42*). Thus, the relatively slow on-rate for chorismate binding (~10^5 M^{-1} s^{-1}) to PhzD can probably be attributed to the unfavorable location of the hydroxyl group on C4 of the cyclohexadiene ring, and is not due to a small population of a sterically favored conformer, or an isomerization step. Additionally, the dissociation constants for chorismate binding to PhzD determined by equilibrium and preequilibrium methods compare favorably, and are in good agreement (Table 3 and

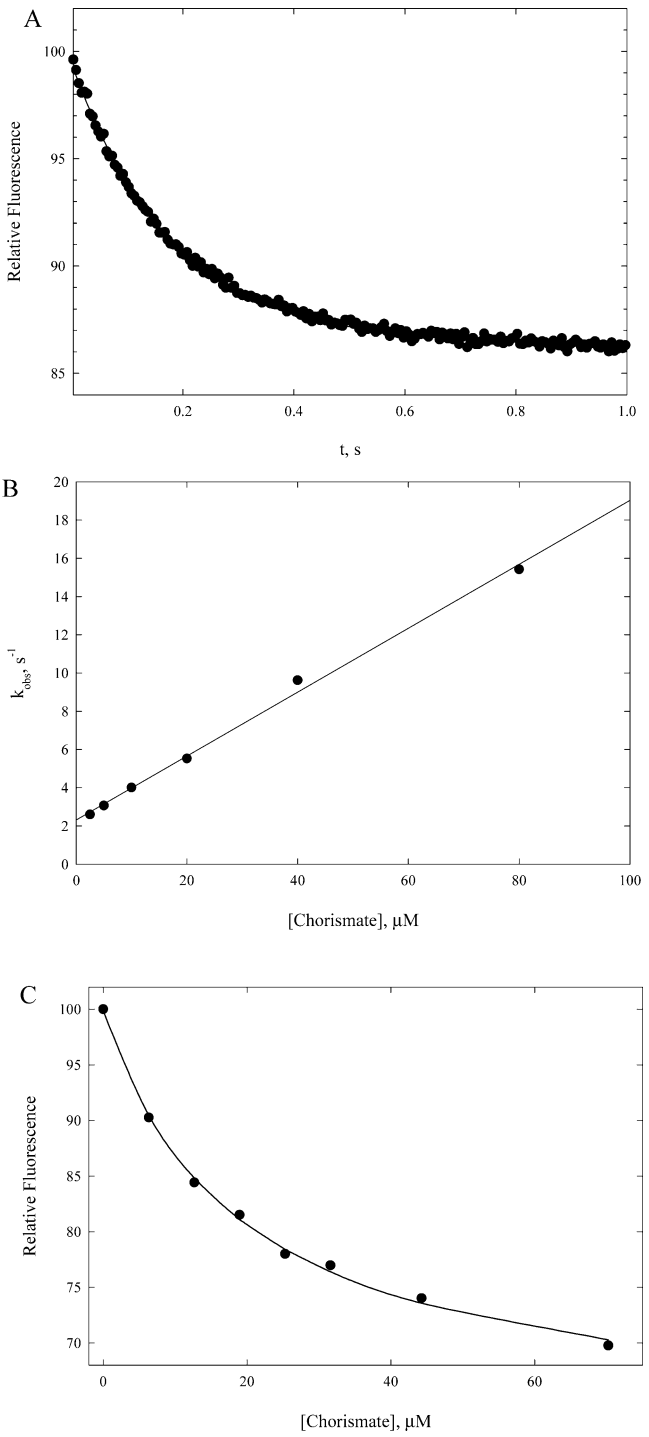

FIGURE 5: Determination of K_d for chorismate binding to D38A PhzD by both the kinetics of the approach to equilibrium and equilibrium titration. (A) Change in protein fluorescence upon rapid mixing of D38A PhzD and chorismate (final concentrations of 0.5 and 20 μM, respectively). Data were fit to a single-exponential decay with a k_{obs} of 5.5 ± 0.16 s^{-1}. (B) Concentration dependence of the observed rate constant for binding of chorismate to D38A PhzD followed by changes in protein fluorescence as depicted in panel A. The solid line is a linear regression fit of the data to eq 2. Values for apparent rate constants are as follows: k_{on} = (1.67 ± 0.03) × 10^5 M^{-1} s^{-1} and k_{off} = 2.3 ± 0.1 s^{-1}. These values yield a K_d of 13.8 ± 2.1 μM. (C) Equilibrium fluorescence intensity as a function of ligand concentration for chorismate binding. The fluorescence emission spectra of 0.5 μM D38A PhzD were measured alone and after additions of chorismate up to 70 μM. Data were fit to a hyperbolic function yielding a K_d of 19.0 ± 1.6 μM, in good agreement with the stopped flow data in panels A and B.

Figures 4 and 5). Rates for ADIC and isochorismate binding to PhzD were too fast to be measured by stopped flow methods. However, these rates can be approximated. If, for example, the off-rates for ADIC and isochorismate are similar to that for chorismate (k_{off} = 2.3 s^{-1}), then the on-rates estimated from the K_d (measured by equilibrium binding) approach the diffusion-controlled limit of ~10^9 M^{-1} s^{-1} for a bimolecular process.

A possible mechanism of vinyl ether hydrolysis catalyzed by PhzD, based on the structure of the D38A−isochorismate complex and the biochemical properties of the enzymes, is presented in Scheme 2. The location of D38 and its proximity to C3′ of the substrate suggest that D38 acts as a general acid in the initial protonation of the substrate in what is probably the slowest chemical step. The resulting carboxylate may further act to stabilize the transiently formed carbocation/oxocarbonium ion. Addition of water to the carbocation yields a hemiketal intermediate. The role of the enzyme in orienting or activating a water molecule is unclear, but the process is fast in any case. Although it is possible that K122 could act as a general base and activate a water molecule to hydrate the carbocation, this process is probably spontaneous since the K122A mutant possesses measurable activity. The hemiketal intermediate also probably decomposes spontaneously to yield products. However, it is again possible that the enzyme plays a role in the process, either in protonating the ether oxygen or in abstracting a proton from the hydroxyl group of the hemiketal. Despite the proximity of the H37 side chain to the pyruvoyl carboxylate, it is the CE1 atom rather than a ring nitrogen that points toward the substrate. Thus, it is unlikely that H37 plays a key role in hemiketal decomposition, but rather that it may be involved in maintaining the proper orientation of D38 or K122. Another possibility for these enzyme-facilitated processes is that D38 could again act as a general acid, protonating the hemiketal ether oxygen, and K122 could then deprotonate the hydroxyl group of the hemiketal. Additional mutagenesis experiments may shed much-needed light on these issues. However, it seems unlikely from the structure that the proton donor is a hydronium ion, as has been proposed previously for the antibody-catalyzed vinyl ether hydrolysis reaction (*43*), because of the anticipated proximity of D38 to C3′ and the body of evidence suggesting vinyl ethers are subject to general acid catalysis at moderate pH (*35*, *44*).

The PhzD−isochorismate structure described here provides the first glimpse of isochorismate bound to an enzyme active site and, therefore, yields interesting clues not only about the mechanism of PhzD but also about the mechanism of some other chorismate-utilizing enzymes. For example, superimposition of native PhzD with the complex of isochorismate with the inactive D38A variant indicates that the initial protonation occurs on one face of the substrate which we have arbitrarily designated *re* (Scheme 2). This observation is consistent with the stereospecific protonation of ADIC reported by Asano et al. (*38*) during the anthranilate synthase reaction. Additionally, the identification of D38 of PhzD as the likely general acid catalyst permits a reexamination of the structure of anthranilate synthase. Spraggon et al. determined the structure of *Serratia marscescens* anthranilate synthase in complex with pyruvate, magnesium, and, surprisingly, benzoic acid (*41*), which was unexpected since there

is no basis for its generation in accepted mechanisms for anthranilate synthase catalysis. However, the location of these ligands allowed identification of the anthranilate synthase active site, which revealed a single acidic residue (E309) as a candidate for protonation of the departing pyruvyl group if, in fact, anthranilate synthase uses a mechanism similar to that of PhzD. Since the protonation has been shown to be stereospecific [on the *re* face (*38*)], it is likely to be part of a concerted reaction along with C2 proton abstraction that results in aromatization of the ring and displacement of the pyruvyl group (Scheme 1). (The general acid need not be an Asp/Glu, of course; in principle Tyr, for example, could also perform the function.) Interestingly, a preliminary model of ADIC bound to the active site of anthranilate synthase suggests that E309 favorably approaches the C3′ group of the intermediate.

The large difference PhzD exhibits in K_d and K_m values may reflect an increased affinity of the substrate for the inactive variant. The structural superimposition of native PhzD with the isochorismate complex suggests that D38 lies close to C3′ of the substrate. Replacement by alanine in the D38A variant eliminates a presumably unfavorable interaction between the methylene carbon and the D38 carboxylate and may provide a more favorable hydrophobic interaction. The weaker binding of chorismate and ADC (Table 3 and Figures 4 and 5) is likely due in part to an unfavorable interaction between the substituent at the 4 position and the side chain of W94. Isochorismate binds in such a way that its cyclohexadiene ring and the indole ring of W94 are stacked against each other (Figure 2A). The C2 OH group of isochorismate is 4.0 Å from the indole nitrogen. If, however, the hydroxyl or amino substituent were on C4, as is the case for chorismate and ADC, an unfavorable interaction would occur between the substituent and the W94 ring. ADC binding would be expected to be particularly poor due to the need to bury the positively charged amino group in a hydrophobic environment.

A comparison of the kinetic data reported here and the data reported previously for the *E. coli* EntB isochorismatase might be expected to provide some additional information regarding recognition of substrates by PhzD and EntB. The kinetic constants for EntB toward isochorismate ($k_{cat} = 10$ s^{-1}, $K_m = 15$ μM) are in reasonable agreement with the data presented in Table 3, although PhzD does exhibit a significantly lower turnover number. Alternatively, PhzD appears to have a greater affinity for chorismate ($K_m \geq 37$ mM with EntB and $K_m \sim 1$ mM with PhzD) (*30*). Interestingly, the authors report that ADIC is neither an inhibitor nor (apparently) a substrate for EntB. They further suggest that the 2-amino group may prevent ADIC binding. Comparison of the primary sequences of EntB and PhzD reveals few significant differences except the previously mentioned C-terminal ACP domain of EntB. In particular, the active site residues of PhzD and EntB are essentially identical. Explaining these differences may require high-resolution structural data on EntB.

PhzD, like other members of the α/β-hydrolase fold family, uses the amino acids positioned on loops following the strands of the core β-sheet as the catalytic machinery (*45*−*47*). The variability seen in the identity of the residues positioned on these loops or "stations" provides the catalytic diversity seen in the α/β-hydrolase superfamily. In the PhzD primary sequence, D38, Q78, K122, and the V150-Y151 *cis* peptide reside on loops 1−4, respectively. The residues following strand β4 often play a key role in defining catalysis and show significant variability across the α/β-hydrolase family. In the case of PhzD, however, it seems likely that a progenitor of PZAase/CSHase was conscripted for duty in phenazine biosynthesis with the primary change being the loss of the cysteine nucleophile. Indeed, a nucleophile is not required for vinyl ether hydrolysis, and in the case of PhzD, any residue except glycine would result in significant steric clashes with the pyruvyl carboxylate portion of the substrate (Figure 2A). The *cis* peptide bond found at the active site of PhzD (following β4), and in each of the proteins listed in Table 2, probably does not function as part of an oxyanion hole to stabilize the intermediate of the PhzD-catalyzed reaction as it likely does for the negatively charged transition states of the PZAase/CSHase reactions (*16*).

On the basis of the limited distribution of the phenazine pathway genes among microbial species, it is possible that *phzD* arose by duplication of *entB*, which encodes an isochorismatase from the more widespread enterobactin pathway. The significant level of identity (46%) between PhzD and EntB supports such a divergent evolutionary relationship. *entB* may have in turn arisen by duplication of *pncA*, which encodes PZAase. Although PZAase is known to be responsible for both susceptibility and resistance to the anti-tuberculosis drug pyrazinamide, its primary metabolic function is the hydrolysis of nicotinamide in the pyrimidine nucleotide pathway. This important function has likely been preserved over time, making PZAase/nicotinamidase a plausible progenitor of PhzD.

ACKNOWLEDGMENT

We are indebted to Gary Gilliland for his interest and support of this work and are grateful to Martin Mayhew, Marcia Holden, Vincent Vilker, Bob Goldberg, and other members of the Bioprocess Engineering Group at the National Institute of Standards and Technology for plasmid DNA, highly purified chorismate, and advice.

REFERENCES

1. Timms-Wilson, T. M., Ellis, R. J., Renwick, A., Rhodes, D. J., Mavrodi, D. V., Weller, D. M., Thomashow, L. S., and Bailey, M. J. (2000) *Plant Microb. Interact. 13*, 1293−1300.
2. Mavrodi, D. V., Ksenzenko, V. N., Bonsall, R. F., Cook, R. J., Boronin, A. M., and Thomashow, L. S. (1998) *J. Bacteriol. 180*, 2541−2548.
3. Mavrodi, D. V., Bonsall, R. F., Delaney, S. M., Soule, M. J., Phillips, G., and Thomashow, L. S. (2001) *J. Bacteriol. 183*, 6454−6465.
4. McDonald, M., Mavrodi, D. V., Thomashow, L. S., and Floss, H. G. (2001) *J. Am. Chem. Soc. 123*, 9459−9460.
5. Usher, L. R., Lawson, R. A., Geary, I., Taylor, C. J., Bingle, C. D., Taylor, G. W., and Whyte, M. K. (2002) *J. Immunol. 168*, 1861−1868.
6. Britigan, B. E., Roeder, T. L., Rasmussen, G. T., Shasby, D. M., McCormick, M. L., and Cox, C. D. (1992) *J. Clin. Invest. 90*, 2187−2196.
7. Kerr, J. R., Taylor, G. W., Rutman, A., Hoiby, N., Cole, P. J., and Wilson, R. (1999) *J. Clin. Pathol. 52*, 385−387.
8. Britigan, B. E., Railsback, M. A., and Cox, C. D. (1999) *Infect. Immun. 67*, 1207−1212.
9. Altschul, S. F., Madden, T. L., Schaffer, A. A., Zhang, J., Zhang, Z., Miller, W., and Lipman, D. J. (1997) *Nucleic Acids Res. 25*, 3389−3402.

10. Gehring, A. M., Mori, I., and Walsh, C. T. (1998) *Biochemistry 37*, 2648−2659.
11. Gehring, A. M., Bradley, K. A., and Walsh, C. T. (1997) *Biochemistry 36*, 8495−8503.
12. Jurkowitz, M. S., Horrocks, L. A., and Litsky, M. L. (1999) *Biochim. Biophys. Acta 1437*, 142−156.
13. Jurkowitz-Alexander, M., Ebata, H., Mills, J. S., Murphy, E. J., and Horrocks, L. A. (1989) *Biochim. Biophys. Acta 1002*, 203−212.
14. Jurkowitz-Alexander, M. S., and Horrocks, L. A. (1991) *Methods Enzymol. 197*, 483−490.
15. Jones, J., and Kresge, A. J. (1993) *Can. J. Chem. 71*, 38−41.
16. Du, X., Wang, W., Kim, R., Yakota, H., Nguyen, H., and Kim, S. H. (2001) *Biochemistry 40*, 14166−14172.
17. Zajc, A., Romao, M. J., Turk, B., and Huber, R. (1996) *J. Mol. Biol. 263*, 269−283.
18. Pflugrath, J. W. (1999) *Acta Crystallogr. D55*, 1718−1725.
19. Terwilliger, T. C., and Berendzen, J. (1999) *Acta Crystallogr. D55*, 849−861.
20. Terwilliger, T. C. (2001) *Acta Crystallogr. D57*, 1755−1762.
21. Terwilliger, T. C. (2001) *Acta Crystallogr. D57*, 1763−1775.
22. Sheldrick, G. M. (1998) in *Direct Methods for Solving Macromolecular Structures* (Dordrecht, F. S., Ed.) pp 401−411, Kluwer Academic Publishers, Dordrecht, The Netherlands.
23. Laskowski, R. A., and MacArthur, M. W. (1993) *J. Appl. Crystallogr. 26*, 283−291.
24. Word, J. M., Lovell, S. C., LaBean, T. H., Taylor, H. C., Zalis, M. E., Presley, B. K., Richardson, J. S., and Richardson, D. C. (1999) *J. Mol. Biol. 285*, 1711−1733.
25. McRee, D. E. (1999) *Practical Protein Crystallography*, 2nd ed., Academic Press, San Diego.
26. Holm, L., and Sander, C. (1995) *Trends Biochem. Sci. 20*, 478−480.
27. Shindyalov, I. N., and Bourne, P. E. (1998) *Protein Eng. 11*, 739−747.
28. Berman, H. M., Wesrbrook, J., Feng, Z., Gilliland, G. L., Bhat, T. N., Weissig, I. N., Shindyalov, P. E., and Bourne, P. E. (2000) *Nucleic Acids Res. 28*, 235−242.
29. Tewari, Y. B., Jensen, P. Y., Kishore, N., Mayhew, M. P., Parsons, J. F., Eisenstein, E., and Goldberg, R. N. (2002) *Biophys. Chem. 96*, 33−51.
30. Rusnak, F., Liu, J., Quinn, N., Berchtold, G. A., and Walsh, C. T. (1990) *Biochemistry 29*, 1425−1435.
31. Morollo, A. A., Finn, M. G., and Bauerle, R. (1993) *J. Am. Chem. Soc. 115*, 816−817.
32. Morollo, A. A., and Bauerle, R. (1993) *Proc. Natl. Acad. Sci. U.S.A. 90*, 9983−9987.
33. Colovos, C., Cascio, D., and Yeates, T. O. (1998) *Structure 6*, 1329−1337.
34. Walsh, C. T., Erion, M. D., Watts, A. E., Delany, J. J., and Berchtold, G. A. (1987) *Biochemistry 26*, 4734−4745.
35. Kresge, A. J., Leibovitch, M., and Sikorski, J. A. (1992) *J. Am. Chem. Soc. 114*, 2618−2622.
36. Walsh, C. T., Liu, J., Rusnak, F., and Sakaitani, M. (1990) *Chem. Rev. 90*, 1105−1130.
37. Kozlowski, M. C., Tom, N. J., Seto, C. T., Sefler, A. M., and Bartlett, P. A. (1995) *J. Am. Chem. Soc. 117*, 2128−2140.
38. Asano, Y., Lee, J. J., Sheih, T. L., Spreafico, C., Kowal, C., and Floss, H. G. (1985) *J. Am. Chem. Soc. 107*, 4314−4320.
39. Knochel, T., Ivens, A., Hester, G., Gonzalez, A., Bauerle, R., Wilmanns, M., Kirschner, K., and Jansonius, J. N. (1999) *Proc. Natl. Acad. Sci. U.S.A. 96*, 9479−9484.
40. Parsons, J. F., Jensen, P. Y., Pachikara, A. S., Howard, A. J., Eisenstein, E., and Ladner, J. E. (2002) *Biochemistry 41*, 2198−2208.
41. Spraggon, G., Kim, C., Nguyen-Huu, X., Yee, M. C., Yanofsky, C., and Mills, S. E. (2001) *Proc. Natl. Acad. Sci. U.S.A. 98*, 6021−6026.
42. Copley, S. D., and Knowles, J. R. (1987) *J. Am. Chem. Soc. 109*, 5008−5013.
43. Reymond, J. L., Jahngiiri, G. K., Stoudt, C., and Lerner, R. L. (1993) *J. Am. Chem. Soc. 115*, 3909−3917.
44. Chwang, W. K., Eliason, R., and Kresge, A. J. (1977) *J. Am. Chem. Soc. 99*, 805−808.
45. Parsons, J. F., Lim, K., Tempczyk, A., Krajewski, W., Eisenstein, E., and Herzberg, O. (2002) *Proteins 46*, 393−404.
46. Morais, M. C., Zhang, W., Baker, A. S., Zhang, G., Dunaway-Mariano, D., and Allen, K. N. (2000) *Biochemistry 39*, 10385−10396.
47. Wang, W., Kim, R., Jancarik, J., Yokota, H., and Kim, S. (2001) *Structure 9*, 65−72.

BI027385D